Title: An Analytical Solution for the Run-out of Submarine Debris flows

Abstract

Submarine debris flows have a significant impact on offshore and coastal facilities. The unique characteristics of submarine debris flows involve large mass movements and long travel distances over very gentle slopes. To improve our insight and knowledge of the basic mechanism behind submarine debris flows, an analytical model was derived for the mobility of submarine debris flows. This model takes into account the mass change of debris flows induced by deposition, stagnation pressure and the topography of the depositional area. One case study on the Palos Verdes debris flow proves its ability to predict the run-out distance of a submarine debris flow to a reasonable level of accuracy. On the gentle slopes, the submarine debris flow progressively loses mass due to deposition, which in turn influence the flow velocity. In addition, the results show that the slope angle and spreading angle of the debris depositional zone play important roles in the sliding process.

Keywords

submarine debris flow, analytical solution, run-out distance, stagnation pressure

List of Notation

P: the stagnation pressure

ρ_w: the density of water

v: the flow velocity

τ_s: the friction force

F': the effective static pressure

ρ_f: the saturated bulk density of debris flow material

β_1: the slope angle of escarpment

$\ddot{u}_{seismic}$: the seismic acceleration

θ: the direction of seismic acceleration

b_0: the initial width of debris flow

λ: the spreading angle of debris deposition zone

β_2: the slope angle of debris deposition zone

L: the length of moving block

σ: the density of particles

D: the diameter of particles

1. Introduction

Submarine debris flows are considered to be one of the most serious geohazards in offshore and coastal areas. Due to the large affected area, even small-scale debris flows in coastal areas can pose severe danger. Coastal infrastructure and populations, and offshore facilities related to resource development and transport facilities, such as pipelines and communication cables, are at risk from submarine debris flows, and must be designed to withstand their impact. An example of submarine cable damage has been found in the Grand Banks debris flow of 1929 where the debris flow and resulting turbidity current broke a series of submarine cables nearly 600 km away from the beginning of the submarine debris flow (Hampton et al., 1996; Mason et al., 2006). Another case of infrastructure destruction occurred when Hurricane Camille hit the Mississippi delta in 1969, causing a debris flow that damaged several offshore drilling platforms (Locat and Lee, 2002).

Submarine debris flows are difficult to observe directly, and so it is difficult to obtain an insight into their behaviour. Many lab experiments have been carried out as small-scale analogues to investigate the roles of slurry properties and water content in debris flow dynamics and depositional structures (Mohrig et al., 1999; Marr et al., 2001; Breien et al., 2007; Boylan et al., 2010; Yin and Rui, 2017; Yin et al., 2018). However, these experiments are usually expensive, and the results are not easily transferable to large-scale conditions. To avoid these issues, a considerable amount of numerical work has been done to use computer models to simulate the failure or sliding of submarine debris flows (Imran et al., 2001; Marr et al., 2001; Gauer et al., 2006; Zhu and Randolph, 2009; Steffen et al., 2008; Pudasaini, 2014; Soundararajan, 2015; Kafle et al. 2016). One early example is the Norem–Irgens–Schieldrop (NIS) model proposed by Norem et al. (1990). The original purpose of the NIS model was to analyse snow avalanches, however through analysis of the results it has been shown that the model is also appropriate for use with submarine debris flows. Later Imran et al. (2001) proposed the BING model, which is developed by incorporation of the Bingham, Herschel-Bulkley and Bilinear rheologies. In the BING model the debris flow motion is considered as two coupled layers that refer to a plug layer and a shear layer. Subsequent research (De Blasio et al., 2005) extended the BING model to be able to calculate run-out behaviour with hydroplaning and shear-wetting. Pudasaini (2012) presented a generalized two-phase debris flow model, which can adequately simulate the complicated dynamics of submarine debris flows and related phenomena. Based on this mode, Kattel et al. (2016) simulated a glacial lake outburst flood, and showed that this model can be applied to simulate particle-fluid flow in conduits that is important for decommissioning of the endangered reservoirs. In addition, Pudasaini (2014) and Kafle et al. (2016) simulated two-phase debris impacting a reservoir, modeling the landslide-induced tsunami, flow transformation, turbidity currents and sediment transports in bathymetric slopes. On the other hand, Mergili et al. (2017, 2018) developed an open source, efficient and high-resolution computational tool (r.avaflow) for routing mass flows from a release area down to a deposition. This innovative tool showed many advantages over other existing tools, such as (i) employment of a two-phase mixture model (Pudasaini, 2012); (ii) capability of modelling complex process chains/interactions; (iii) modelling of multiple release masses and/or hydrographs.

Although numerical models can offer a more accurate and detailed method of modelling flow dynamics, there are also some limitations to these numerical techniques, such as the amount of computing power needed and possible calculation errors. Other studies include empirical, semi-empirical and analytical modelling based on field observations and experimental data. Hampton et al. (1996) proposed that submarine debris flows can be described using rigid body or continuum models. De Blasio et al. (2006) focused on the extraordinary mobility of submarine debris flows, and concluded that the run-out ratios of vertical fall height to horizontal travel distance may reach values as low as 0.05–0.01. Legros (2002) proposed another closed solution for the mobility of long run-out debris flows, which indicates that the debris flow spreading is essentially controlled by the volume, not the fall height. Boukpeti et al. (2012) presented analytical models for different rheological models of the debris flow material, but no solution was given and the run-out distance was not discussed. In addition, Pudasaini and Miller (2013) presented a mass or volume dependent model for hypermobility of huge landslides and avalanches. The model can be used to estimate the overrun area and volume in terms of known mobility data.

Generally, analytical solutions for submarine debris flows require simplification of some conditions by making assumptions on flow dynamics, since it is not possible to solve complicated questions involving uncertain characteristics of soil/rock sediments, the geometrical complexity of the sea bed, the interaction between a debris flow and the ambient water, and the complicated mechanism behind sliding. However, these investigations are widely considered to be important because they help to clarify the fundamental characteristics of the phenomenon, and improve our insight and knowledge of the basic mechanism behind submarine debris flows (Tinti and Bortolucci, 2000). This paper discusses and develops an analytical approach to the run-out distance of submarine debris flows. This approach has taken into account the impacts of mass change, stagnation pressure and depositional shape.

2. An analytical model for the submarine debris flow dynamics

Submarine debris flows describe the downward movement of a disturbed mass, after shear failure on the sliding surfaces. The disturbed mass travels down the slope in different manners according to the material attributes, topography and boundary conditions. Accordingly, the mobility behaviour of submarine debris flows can be divided into two categories. On a steep slope, the component of gravity in the downslope direction is usually larger than the friction between the moving mass and the base of the slope, and the mass of the whole submarine debris flow body remains constant without leaving deposits, as shown in

Figure 1. Similar assumptions could be found in the analytical model by Hürlimann et al. (2000). On a gentle slope, due to the basal friction being higher than the component of gravity force downslope, the material at the bottom of the displaced mass decelerates quickly until completely stopped, but the upper part of the mass still moves downwards due to inertia. Such depositional behaviours have also been simulated and shown with analytical models by Legros (2002), Pudasaini and Kroener (2008), and Pudasaini (2011). This process indicates deposition at the base of the debris flow, which thus progressively runs out of all of the material. The mechanisms for submarine debris flows on steep and gentle slopes are quite different, and hence two analytical models are needed for these two different cases.

Figure 1. Evolution of a submarine debris flow.

2.1 Constant-mass model

In the first model, the height and volume of debris flow are assumed to remain constant through the flow process. Hence, this simplified model is called constant-mass model. Once failure occurs, it is assumed that the debris flow comprises a homogenous mass which moves over a fixed slope. On a steep slope, when the displaced mass has sufficient strength, the submarine debris flow may avoid fragmentation and remain as one single body. Considering the simplified process of a submarine debris flow as represented in Figure 2, several assumptions are made: (a) the debris flow is considered to have a constant mass, and (b) the height, length and width of the debris flow remain constant during the flow process (means it does not deposit).

Figure 2. Schematic of a submarine debris flow (mass conservation) where Xmax = maximum distance travelled.

The driving forces acting on the debris flow are proportional to the gravitational acceleration component parallel to the slope bed. Opposing these forces, as shown in Figure 2, are the friction with the slope bed and the drag force due to the surrounding fluid, caused by the stagnation pressure (De Blasio, et.al, 2004). From Bernoulli's principle, the stagnation pressure is given by:

$$\mathrm{P} = \frac{1}{2}\rho_w v^2, \tag{1}$$

where ρ_w is the water density and v is the flow velocity of submarine debris. The friction between the debris flow and the bed surface is assumed to follow classical Coulomb law, and therefore can be presented as:

$$\mathrm{T} = \mathrm{F}' \cdot \tan\alpha\ , \tag{2}$$

where T is the friction force between the debris flow and the bed surface, F' is the effective static pressure due the overburden with consideration of buoyancy, and α is the friction angle, considering the effects of water as a fluidized medium. (Pudasaini and Miller, 2013) The effective static pressure, F' can be expressed as:

$$\mathrm{F}' = (\rho_f - \rho_w)\mathrm{g}\mathrm{V}\cos\beta, \tag{3}$$

where ρ_f is the density of the sliding material, h is its height, and β is the slope angle, V is the volume of the moving block, and V≈b· $\mathrm{h}\cdot\mathrm{l}$ (width, height and length of moving block). The gravity component of the force in the downslope direction with consideration of buoyancy is:

$$\mathrm{G}_x' = (\rho_f - \rho_w)\ \mathrm{g}\mathrm{V}\sin\beta. \tag{4}$$

Accordingly, based on the conservation of energy, the debris flow mechanics can be approximated by the following equation:

$$\mathrm{dE} = \mathrm{F}_j \cdot \mathrm{dx}, \tag{5}$$

where F_j is the net driving force given by (1), (2) and (4), x is the flow displacement, and E is the kinetic energy.

$$\mathrm{F}_j = \mathrm{G}_x' - \mathrm{T} - \mathrm{P}\cdot\mathrm{hb}, \tag{6}$$

$$E = \frac{1}{2}\mathrm{m}v^2. \tag{7}$$

Hence, for constant m, equation (5) can be expanded as:

$$\mathrm{m}v\frac{\mathrm{d}v}{\mathrm{dx}} = \mathrm{m}'\mathrm{g}\sin\beta\ - \mathrm{m}'\mathrm{g}\cos\beta\tan\alpha - \frac{1}{2}\rho_w v^2\mathrm{hb}, \tag{8}$$

where the mass of the sliding material, $\mathrm{m} = \rho_f\mathrm{blh}$, $\mathrm{m}' = (\rho_f - \rho_w)\mathrm{blh}$. This can be simplified to:

$$v\frac{\mathrm{d}v}{\mathrm{dx}} = \mathrm{g}\frac{\rho_f - \rho_w}{\rho_f}\sin\beta - \frac{\rho_f - \rho_w}{\rho_f}\mathrm{g}\cos\beta\tan\alpha\ - \frac{1}{2l}\frac{\rho_w}{\rho_f}v^2. \tag{9}$$

Equation (9) can be expressed in the form:

$$\frac{d(v^2)}{dx} = A - Bv^2, \quad (10)$$

where:

$$A = 2\frac{\rho_f - \rho_w}{\rho_f} g\sin\beta - 2\frac{\rho_f - \rho_w}{\rho_f} g\cos\beta \tan\alpha, \quad (11)$$

$$B = \frac{\rho_w}{\rho_f l}. \quad (12)$$

This simplified constant-mass model is also mentioned by Hürlimann et al. (2000). The difference is that Hürlimann's model is derived based on Newton's second law. In some cases where the submarine debris flows are induced by the earthquake, the effect of the seismic load on the moving mass needs to be included. This seismic load can be simplified as the product of mass times constant seismic acceleration, $\ddot{u}_{seismic}$, in the direction of θ. This seismic load is applied to the moving mass, as shown in Figure 2. Hence A can be expressed as:

$$A = 2\frac{\rho_f - \rho_w}{\rho_f} g\sin\beta + 2\ddot{u}_{seismic}\cos(\theta - \beta) - 2\frac{\rho_f - \rho_w}{\rho_f} g\cos\beta \tan\alpha - 2\ddot{u}_{seismic}\sin(\theta - \beta)\tan\alpha.$$

(13)

The flow displacement is obtained by integrating Equation (10) between X_0 and X_i which correspond to the velocities v_0 and v_i, respectively:

$$-\frac{1}{B}\ln(A - Bv^2) = X_i - X_0 \qquad \Big|_{v_0}^{v_i} \quad (14)$$

Accordingly, if the initial flow velocity is known, Equation (15) can be used to predict the value of the velocity after a certain flow displacement.

2.2 Changing-mass model

During the run-out process the debris flow mass may change, due to deposition of material or accretion of material from the bed, which is the case in general during erosion and deposition process (Pudasaini and Fischer, 2016). Cannon and Savage (1988), Gassen and Cruden, (1989), and Voight and Sousa (1994) showed that the impact of progressive changes to mass due to deposition will increase the run-out distance of debris flow. Therefore, we may wonder whether a debris flow that progressively loses mass due to deposition might not maintain a higher velocity and travel further than a debris flow that moves and stops as a single block (Legros, 2002; Pudasaini and Fischer 2016). According to this assumption, as presented in Figure 3, mass loss occurs at some point where the debris flow starts to deposit material, and only the upper part of debris proceed in the flow regime. Hence, a deposition model, which could be used to simulate the erosion and spreading behaviour of submarine debris flow, needs to be introduced. Pudasaini and Fischer (2016) indicated that the deposition models can be divided into two categories: empirical and mechanical ones. Empirical model is always calibrated by specific case and hence become case dependent. Process-based mechanical models are based on the mass and momentum exchanges between the slope bed and sliding debris, and the magnitude of erosion rate is shows a proportional relationship with the shear stress difference between entraining and resisting stresses.(Iverson, 2012; Issler, 2014). Within this framework, Legros (2002) proposed a deposition model, in which the thickness of the upper part of debris which still proceed in the flow regime was expressed as,

$$\mathrm{h} = \frac{f_c \sigma D^2 cos\alpha}{\rho_f g}\left(\frac{\mathrm{dv}}{dy}\right)^2 , \tag{15}$$

where σ is the density of particles, D is the diameter, f_c is a positive function of the particle concentration.

Assuming that dv/dy = v/h_s, where h_s is the typical thickness of the shearing zone, Legros (2002) simplified Equation (15) into

$$\mathrm{h} = \frac{f_c \sigma D^2 cos\alpha}{\rho_f g h_s^2} v^2 = \mathrm{B}_1 v^2 , \tag{16}$$

where B_1 is the material constant, which is dependent on granular concentration, grain diameter, density of particles and dispersive pressure. All the parameters in Equation 16 is assumed independent of v. On the other hand, equation (16) has also been derived analytically in Pudasaini (2011) in which the constant coefficient is explicitly expressed in terms of the mechanical and material parameters. It should be noted that mass loss is only represented in this model by a rebhnduction in flow height, and not in a real extent. (Legros, 2002).

Figure 3. Schematic of a submarine debris flow run-out that includes transformation from the constant-mass model to the non-constant-mass model.

By assuming that the area, $(s = bl)$, of the moving debris flow does not vary with time (Legros, 2002), and that $m = blh\rho_f$, therefore:

$$dm = \mathrm{bl}\rho_\mathrm{f} \cdot \mathrm{dh}. \tag{17}$$

This assumption restricts the analytical model. However, Legros (2002) compared this assumption and three cases of natural landslides, which shows the errors induced by this assumption are acceptable. In addition, the results of some numerical simulations (Campbell et al. 1995) also confirm this assumption.

Combing equation (5), (6) and (7):

$$\frac{d(\frac{1}{2}mv^2)}{dx} = G - T - P\mathrm{hb}. \tag{18}$$

Substituting equations (1), (2) and (4) into Equation (18):

$$\frac{v^2 dm}{2dx} + \frac{mvdv}{dx} = \mathrm{m}' \ \mathrm{g}\sin\beta - \mathrm{m}' \ \mathrm{g}\cdot\tan\alpha\cos\beta \ - \frac{1}{2}\rho_\mathrm{w}\mathrm{v}^2\mathrm{hb}. \tag{19}$$

The length of the moving mass, l, is also a variable based on the debris flow spreading in the horizontal direction. This debris flow spreading may be very complicated due to the complexity of the local topography, but it can be simplified as a radially spread deposit, as shown in Figure 4. The width of the moving mass can be written as $\mathrm{b(x)} = \mathrm{b}_0 + \lambda\mathrm{x}$, where b_0 is the initial width and λ is the spreading angle. Hence, the length of the moving mass $\mathrm{l(x)} = \mathrm{s}/(\mathrm{b}_0 + \lambda\mathrm{x})$.

(a) (b)

Figure 4. Plan view schematic of a debris flow on a gentle slope.

Equation (19) can be rewritten as:

$$\frac{v^2}{2h}\frac{dh}{dx} + v\frac{dv}{dx} = -\tan\alpha\cos\beta\frac{\rho_f-\rho_w}{\rho_f}g - \frac{1}{2}\frac{\rho_w}{\rho_f}v^2\frac{b_0+\lambda x}{s} + \frac{\rho_f-\rho_w}{\rho_f}g\sin\beta. \tag{20}$$

It is essential to this model that the value of h changes with the debris flow, as described in Equation 16. It is noted that B_1 is eliminated when substituting Equation (16) into Equation (20), and hence it avoid the determination of those complicated parameters. Therefore Equation (20) can be expressed in the form:

$$\frac{d(v^2)}{dx} + M + N(b_0 + \lambda x)v^2 = 0, \tag{21}$$

where, $N = \frac{\rho_w}{2\rho_f s}$, $M = \tan\alpha \times \cos\beta\frac{\rho_f-\rho_w}{\rho_f}g - \frac{\rho_f-\rho_w}{\rho_f}g\sin\beta$, which can also include the seismic load.

Therefore, a closed-form solution of Equation (21) can be expressed as:

$$v^2 = Ce^{-N\left(b_0x+\frac{1}{2}\lambda x^2\right)} + e^{-N\left(b_0x+\frac{1}{2}\lambda x^2\right)}\frac{M\sqrt{\pi}\times i\times e^{-\frac{b_0{}^2N}{2\lambda}}\mathrm{erf}\left(\frac{\sqrt{2N}(b_0+x\lambda)\times i}{2\sqrt{\lambda}}\right)}{\sqrt{2N\lambda}}, \tag{22}$$

where C is a constant, which can be calculated by the initial condition and $i = \sqrt{-1}$.

The run-out distance X_{max} at which v becomes zero can be obtained implicitly by solving the equation as:

$$Ce^{-N\left(b_0x+\frac{1}{2}\lambda x^2\right)} + e^{-N\left(b_0x+\frac{1}{2}\lambda x^2\right)}\frac{M\sqrt{\pi}\times i\times e^{-\frac{b_0{}^2N}{2\lambda}}\mathrm{erf}\left(\frac{\sqrt{2N}(b_0+x\lambda)\times i}{2\sqrt{\lambda}}\right)}{\sqrt{2N\lambda}} = 0. \tag{23}$$

On the other hand, if the mass-changing model (Equation 16) which describes the erosion-deposition behaviour is not considered, Equation (19) can be written as,

$$\frac{1}{2}\cdot\frac{d(v^2)}{dx} = -\tan\alpha\cos\beta\frac{\rho_f-\rho_w}{\rho_f}g + \frac{\rho_f-\rho_w}{\rho_f}g\sin\beta - \frac{\rho_w}{2\rho_f}\frac{b_0+\lambda x}{s}v^2. \tag{24}$$

Accordingly, the final solution of debris flow velocity without considering mass-changing can be rewritten. So, essentially the mapping $N \to N/2$ was from none-mass-changing solution to mass-changing solution,

$$v^2 = Ce^{-2N\left(b_0x+\frac{1}{2}\lambda x^2\right)} + e^{-2N\left(b_0x+\frac{1}{2}\lambda x^2\right)}\frac{M\sqrt{\pi}\times i\times e^{-b_0{}^2\frac{N}{\lambda}}\mathrm{erf}\left(\frac{\sqrt{N}(b_0+x\lambda)\times i}{\sqrt{\lambda}}\right)}{\sqrt{N\lambda}}. \tag{25}$$

3. Application of analytical models

The proposed analytical model was used to analyse a well-known event: the Palos Verdes debris flow (Hampton et al., 1996; Locat and Lee, 2002; Locat et al., 2004), located on the continental slope near Los Angeles. Based on seismic reflection logs of the local morphology, the feature of the sea floor lying at the base of the escarpment was recognised as a submarine rock avalanche (Gorsline et al. 1984). The debris avalanche deposit at the toe of the escarpment resulted from a failure that took place along the upper part of the escarpment. The morphology of the escarpment is described in Figure 5. The slope of the escarpment varies between 10° and 17°. At the toe of the escarpment, the debris avalanche deposit spread for a distance of about 8 km, over a slope varying between 1.5° and 2°. The Palos Verdes debris flow process can be divided into two different stages, according to the material attributes and topography. The first stage refers to a constant-mass debris flow process on the escarpment (failure plane). The debris flow is simplified as a whole block with constant mass for the whole sliding process. The sliding distance is about 1km, as shown in Figure 5. Due to the variety of slope, the calculation is divided into 10 steps, referring to 10 sections of escarpment in Figure 5(b). In this process, the spreading angle λ is assumed as 0°, and hence the width b of moving block always equals to the initial value 1000m. Other parameters are listed in Table 1 and Table 2. The initial velocity v_0 is $0\mathrm{m}/s$, and the final velocity in section one $\mathrm{v}_{0.1\mathrm{km}}$ (velocity at distance of 0.1km) can be calculated by Equation 14. This velocity $\mathrm{v}_{0.1\mathrm{km}}$ would be the initial velocity in the next step. Repeating this calculation could get the final velocity of constant-mass debris flow $\mathrm{v}_{1\mathrm{km}}$, defined as the velocity at the toe of the escarpment and initial velocity of deposit zone. The second stage refers to the debris flow in which debris flow was deposited in the debris deposit zone (section 11 in Figure 5(b)). The debris flow is simplified as a whole block as well, but with varying mass. The final sliding distance x_{final} can be calculated by solving Equation (23). The change in the slope of deposit zone is very limited, hence the deposit zone is treated as one whole section. In this model, the the basal topography changes with the changing mass is not considered, which may influence the entire flow dynamics. Hence, the future work will focus on the implementation of the full mechanical models (Pudasaini and Fischer, 2016; Mergili et al., 2017, 2018).

(a) (b)

Figure 5. San Pedro Escarpment and the Palos Verdes avalanche deposit: (a) plan view (Google map, 2017); (b) side view (after Locat et al., 2004).

Table 1 Geometry of escarpment for the Palos Verdes debris flow.

Locat et al. (2004) conducted a numerical analysis of the mobility of the Palos Verdes debris avalanche. The analysis of the failure stage indicated that the debris avalanche was caused by a major earthquake with a magnitude around 7 on the Richter scale, corresponding to a seismic acceleration of 0.3–0.4 g in the downslope direction, where g is the gravitational acceleration. Some of the other parameters from Locat et al. (2004) for the Palos Verdes debris flow were also used in the analytical model, and are listed in Table 2. The variety in the value of average slope angle of escarpment, slope and spreading angle of debris deposition zone is used for parametric study.

Table 2 Parameters for analysis of the Palos Verdes debris flow.

The above values listed in Table 2 were applied to the analysis. The results are given in Figure 6, with the dash line indicating the most probable values for the real situation about 8km. (Locat et al., 2004) The figure shows that most of the results are close to the real value. Most of the relative errors are below 20%. Hence it demonstrates the ability of the analytical solution to predict the run-out distance of a submarine debris flow to a reasonable level of accuracy. Figure 6(a) shows the prediction of the run-out distance with varying slope angles for the escarpment and debris deposition zone. It is shown that the run-out distance increases with increase in either the average slope angle of the escarpment, β_1, or the angle of the debris deposition zone, β_2. When $\beta_2 = 2°$, variations of β_1 from 10° to 17° lead to an increase in the run-out distance from about 7.9 km to 9.5 km. On the other hand, as β_2 increases from 1.5° to 2°, the average change in the run-out distance of all the cases is about 2 km. Therefore, this result indicates that β_2 has a greater influence on the overall run-out distance than β_1. Figure 6(b) shows the prediction of the run-out distance with varying escarpment slope angles and spreading angles of the debris deposition zone. The effect of the spreading angle of debris deposition zone on the run-out distance was investigated, showing an inverse relationship between the run-out distance and the spreading angle of the debris deposition zone. A larger spreading angle, λ, causes a larger width of the moving mass, and hence a comparatively larger stagnation pressure applied to the front of the moving mass. Therefore, the overall run-out distance decreases when the spreading angle, λ, increases. In addition, in order to estimate the effect of mass-changing model, which is described in Equation (16), a sensitivity analysis has been performed as shown in Figure 6(c). Equation (25) describes this simplified model. It is shown that the calculated run-out distance decreased about 40% in all cases when the mass-changing model is not considered. Therefore, it can be concluded that mass-changing and deposition play important roles in the extraordinary mobility of submarine debris flow. However, the present model cannot explain the mechanism for why reduction of sliding mass results in increased mobility. The two-phase mechanical erosion-deposition model by Pudasaini and Fischer (2016) proved that erosion enhances flow mobility, while deposition reduces mobility.

(a) (b) (c)

Figure 6. Calculated run-out distance: (a) with varying slope angles of the escarpment and the debris deposition zone; (b) with varying escarpment slope angles and spreading angles of the debris deposition zone; (c) with and without considering the mass changing model.

4. Conclusions

This paper has presented analytical solutions for determining the run-out distance of a submarine debris flow, with the aim of exploring the sensitivity of the results to different geomechanical attributes and environmental factors. The following conclusions are derived:

(1) The analytical solutions proposed in this paper consider the erosion and spreading behaviour of submarine debris flows, and hence are able to predict the run-out distance of submarine debris flows to a reasonable level of accuracy.

(2) If the debris flow material has sufficient shear strength, the moving block may avoid fragmentation and remain as one single body on a steep sliding surface. However, debris deposition occurs on gentle slopes. The debris flow material progressively loses mass due to deposition, which has a large influence on the flow velocity. It is shown that the calculated run-out distance decreased about 40% when neglecting the mass-changing model. But its mechanical significance still needs future research to be prove, because it contradicts with the mechanically derived model by Pudasaini and Fischer (2016) which clearly shows that only relatively increased friction leads to deposition.

(3) Water is an important factor for submarine debris flows. It not only affects the friction angle as a fluidising medium, but also applies stagnation pressure to the moving block. The additional resistance from water leads to a decrease in velocity, and hence a decrease of the final run-out distance of the submarine debris flow.

(4) The run-out distance of submarine is primarily controlled by the local slope of the depositional zone. This affect is much larger than that from the angle of the escarpment slope.

(5) There is an inverse relationship between the run-out distance and the spreading angle of the debris deposition zone, since the increase in the stagnation pressure induced by the spreading of the deposition zone.

Acknowledgement

This research work is part of the activities of the Schofield Centre at University of Cambridge. The work presented in the paper is part of the Modelling of Mudslide Runout Project which was a collaborative project between University of Cambridge and BP.

We thank Dr. Stuart Haigh, (University of Cambridge) and Professor Kenichi Soga, (UC Berkeley) for comments that greatly improved the research results, and Mr Takaaki Kobayashi for the assistance with the whole project. We would also like to show our gratitude to Dr. Paul Dimmock (BP) for fully supporting this project and sharing his pearls of wisdom with us during the collaboration.

Reference

Boukpeti, N., White, D. J., Randolph, M. F., & Low, H. E. (2012). Strength of fijkne-grained soils at the solid–fluid transition. Geotechnique 62, No. 3, pp. 213–226.

Boylan, N., Gaudin, C., White, D.J., & Randolph, M. F. (2010). Modelling of submarine slides in the geotechnical centrifuge. 7th Int. Conf. on Physical Modelling in Geotechnics (ICPMG). Zurich. 1095-1100.

Breien, H., Pagliardi, M., Blasio, F., Issler, D., & Elverhшi, A. (2007). Experimental studies of subaqueous vs. subaerial debris flows–velocity characteristics as a function of the ambient fluid. Submarine Mass Movements and Their Consequences, pp. 101--110.

Campbell, C. S., Cleary, P. W., & Hopkins, M. (1995). Large-scale landslide simulations: Global deformation, velocities and basal friction. Journal of Geophysical Research: Solid Earth, 100(B5), 8267-8283.

Cannon, S. H., & Savage, W. Z. (1988). A mass-change model for the estimation of debris-flow runout. The Journal of Geology, 221-227.

De Blasio, F. V., Engvik, L., Harbitz, C. B., & Elverhøi, A. (2004). Hydroplaning and submarine debris flows. Journal of Geophysical Research: Oceans (1978–2012), 109(C1).

De Blasio, F. V., Elverhøi, A., Issler, D., Harbitz, C. B., Bryn, P., & Lien, R. (2005). On the dynamics of subaqueous clay rich gravity mass flows—the giant Storegga slide, Norway. Marine and Petroleum Geology, 22(1), 179-186.

De Blasio, F. V., Elverhoi, A., Engvik, L. E., Issler, D., Gauer, P., & Harbitz, C. (2006). Understanding the high mobility of subaqueous debris flows.NORSK GEOLOGISK TIDSSKRIFT, 86(3), 275.

Gassen, W. V., & Cruden, D. M. (1989). Momentum transfer and friction in the debris of rock avalanches. Canadian Geotechnical Journal, 26(4), 623-628.

Gauer, P., Elverhoi, A., Issler, D., & De Blasio, F. V. (2006). On numerical simulations of subaqueous slides: back-calculations of laboratory experiments of clay-rich slides. NORSK GEOLOGISK TIDSSKRIFT, 86(3), 295.

GOOGLE MAPS, 2017. Map of San Pedro Escarpment: Undersea Features. [online]. Google. Available from: http://www.geographic.org/geographic_names/name.php?uni=-241460&fid=6437&c=undersea_features [Accessed 1May 2017].

Gorsline, D. S., Kolpack, R. L., Karl, H. A., Drake, D. E., Thornton, S. E., Schwalbach, J. R., ... & Fleischer, P. (1984). Studies of fine-grained sediment transport processes and products in the California Continental Borderland. *Geological Society, London, Special Publications*, 15(1), 395-415.

Hampton, M., Lee, H., & Locat, J. (1996). Submarine landslides. Reviews of Geophysics 34(1), pp. 33--59.

Hürlimann, M., Garcia-Piera, J. O., & Ledesma, A. (2000). Causes and mobility of large volcanic landslides: application to Tenerife, Canary Islands. *Journal of Volcanology and Geothermal* Research, 103(1-4), 121-134.

Imran, J., Harff, P. and Parker, G. (2001). A numerical model of submarine debris flow with graphical user interface. Computers & Geosciences, 27: 717-729.

Issler, D. (2014). Dynamically consistent entrainment laws for depth-averaged avalanche models. *Journal of Fluid Mechanics*, 759, 701-738.Iverson, R. M. (1997). The physics of debris flows. Reviews of geophysics, 35(3), 245-296.

Iverson, R. M. (2012). Elementary theory of bed - sediment entrainment by debris flows and avalanches. *Journal of Geophysical Research: Earth Surface*, 117(F3).

Kafle, J., Pokhrel, P. R., Khattri, K. B., Kattel, P., Tuladhar, B. M., & Pudasaini, S. P. (2016). Landslide-generated tsunami and particle transport in mountain lakes and reservoirs. *Annals of Glaciology*, 57(71), 232-244.

Kattel, P., Khattri, K. B., Pokhrel, P. R., Kafle, J., Tuladhar, B. M., & Pudasaini, S. P. (2016). Simulating glacial lake outburst floods with a two-phase mass flow model. *Annals of Glaciology*, *57*(71), 349-358.

Legros, F. (2002). The mobility of long-runout landslides. Engineering Geology, 63(3), 301-331.

Locat, J., & Lee, H. J. (2002). Submarine landslides: advances and challenges. Canadian Geotechnical Journal, 39(1), 193-212.

Locat, J., Lee, H. J., Locat, P., & Imran, J. (2004). Numerical analysis of the mobility of the Palos Verdes debris avalanche, California, and its implication for the generation of tsunamis. Marine Geology, 203(3), 269-280.

Marr, J., Harff, P., Shanmugam, G., & Parker, G. (2001), Experiments on subaqueous sandy gravity flows: The role of clay and water content in flow dynamics and depositional structures. Geological Society of America Bulletin 113(11), pp. 1377.

Masson, D., Harbitz, C., Wynn, R., Pederson, G., & Lovholt, F. (2006). Submarine landslides: processes, triggers and hazard protection. Philosophical Transactions of the Royal Society, 364, 2009-2039.

Mergili, M., Jan-Thomas, F., Krenn, J., & Pudasaini, S. P. (2017). r. avaflow v1, an advanced open-source computational framework for the propagation and interaction of two-phase mass flows. Geoscientific Model Development, 10(2), 553.

Mergili, M., Emmer, A., Juřicová, A., Cochachin, A., Fischer, J. T., Huggel, C., & Pudasaini, S. P. (2018). How well can we simulate complex hydro-geomorphic process chains? The 2012 multi-lake outburst flood in the Santa Cruz Valley (Cordillera Blanca, Perú). Earth Surface Processes and Landforms.

Mohrig, D., Elverhøi, A., & Parker, G. (1999). Experiments on the relative mobility of muddy subaqueous and subaerial debris flows, and their capacity to remobilize antecedent deposits. Marine Geology, 154(1), 117-129.

Marr, J. G., Elverhøi, A., Harbitz, C., Imran, J., & Harff, P. (2002). Numerical simulation of mud-rich subaqueous debris flows on the glacially active margins of the Svalbard–Barents Sea. Marine Geology, 188(3), 351-364.

Norem, H., Locat, J., & Schieldrop, B. (1990). An approach to the physics and the modeling of submarine flowslides. *Marine Georesources & Geotechnology* 9(2), 93—111.

Pudasaini, S. P., & Kröner, C. (2008). Shock waves in rapid flows of dense granular materials: Theoretical predictions and experimental results. *Physical Review E*, *78*(4), 041308.

Pudasaini, S. P. (2011). Some exact solutions for debris and avalanche flows. *Physics of Fluids*, *23*(4), 043301.

Pudasaini, S. P. (2012). A general two‐phase debris flow model. *Journal of Geophysical Research: Earth Surface*, *117*(F3).

Pudasaini, S. P., & Miller, S. A. (2013). The hypermobility of huge landslides and avalanches. *Engineering Geology*, *157*, 124-132.

Pudasaini, S. P. (2014). Dynamics of submarine debris flow and tsunami. *Acta Mechanica*, 225(8), 2423-2434.

Pudasaini, S. P., & Fischer, J. T. (2016). A mechanical erosion model for two-phase mass flows. *arXiv preprint arXiv:1610.01806*.

Soundararajan, K. K. (2015). Multi-scale multiphase modelling of granular flows. PhD Thesis, University of Cambridge, UK.

Steffen, M., Kirby, R. M., & Berzins, M. (2008). Analysis and reduction of quadrature errors in the material point method (MPM). International Journal for Numerical Methods in Engineering, 76(6), 922-948.

Tinti, S., & Bortolucci, E. (2000). Analytical investigation on tsunamis generated by submarine slides.

Voight, B., & Sousa, J. (1994). Lessons from Ontake-san: a comparative analysis of debris avalanche dynamics. Engineering Geology, 38(3), 261-297.

Yin, M., & Rui, Y. (2017). Laboratory study on submarine debris flow. *Marine Georesources & Geotechnology*, 1-9.

Yin, M., Rui, Y., & Xue, Y. (2017). Centrifuge study on the runout distance of submarine debris flows. *Marine Georesources & Geotechnology*, 1-11.

Zhu, H., & Randolph, M. F. (2009). Large deformation finite-element analysis of submarine landslide interaction with embedded pipelines. International Journal of Geomechanics.

Figure captions

Figure 1 Evolution of a submarine debris flow

Figure 2 Schematic of a slide (mass conservation) where Xmax = maximum distance travelled

Figure 3 Schematic of a submarine debris flow run-out that includes transformation from the constant-mass model to the non-constant-mass model

Figure 4 Plan view schematic of a slide on a gentle slope

Figure 5. San Pedro Escarpment and the Palos Verdes avalanche deposit: (a) plan view (Google map, 2017); (b) side view (after Locat et al., 2004)

Figure 6 Calculated run-out distance: (a) with varying slope angles of the escarpment and the debris deposition zone; (b) with varying escarpment slope angles and spreading angles of the debris deposition zone; (c) with and without considering the mass changing model

Table captions

Table 1 Geometry of escarpment

Table 2 Parameters for analysis of the Palos Verdes slide

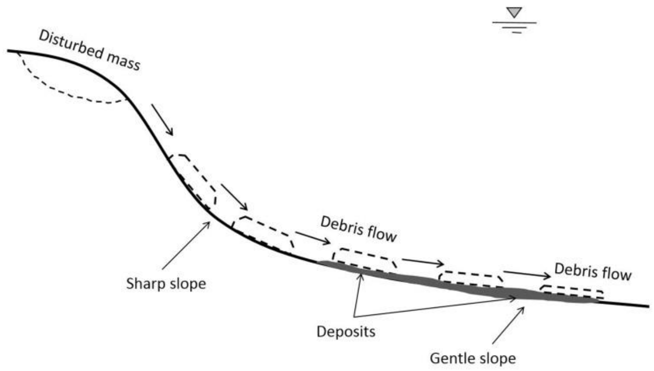

Figure 1. Evolution of a submarine debris flow

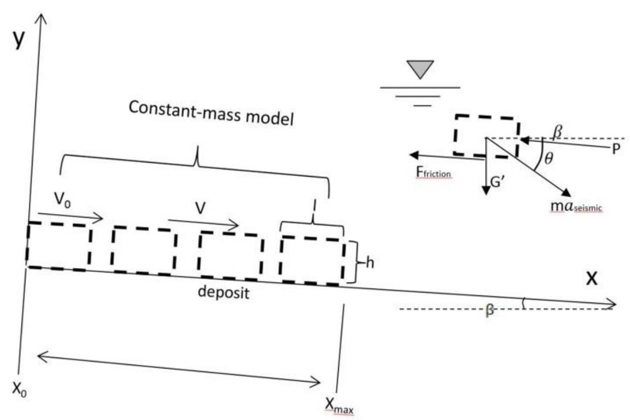

Figure 2. Schematic of a submarine debris flow (mass conservation) where X_{max} = maximum distance travelled

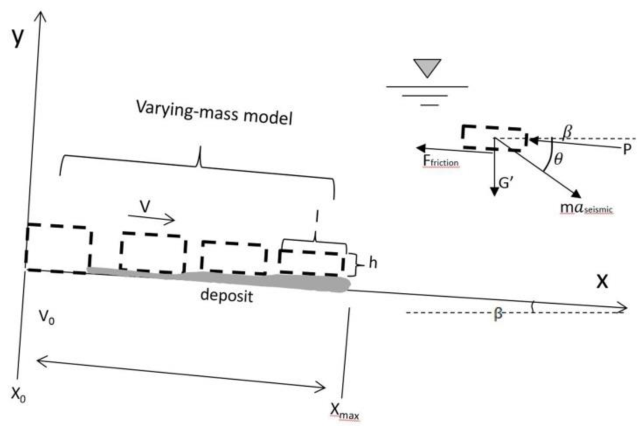

Figure 3. Schematic of a submarine debris flow run-out that includes transformation from the constant-mass model to the non-constant-mass model

(a) (b)

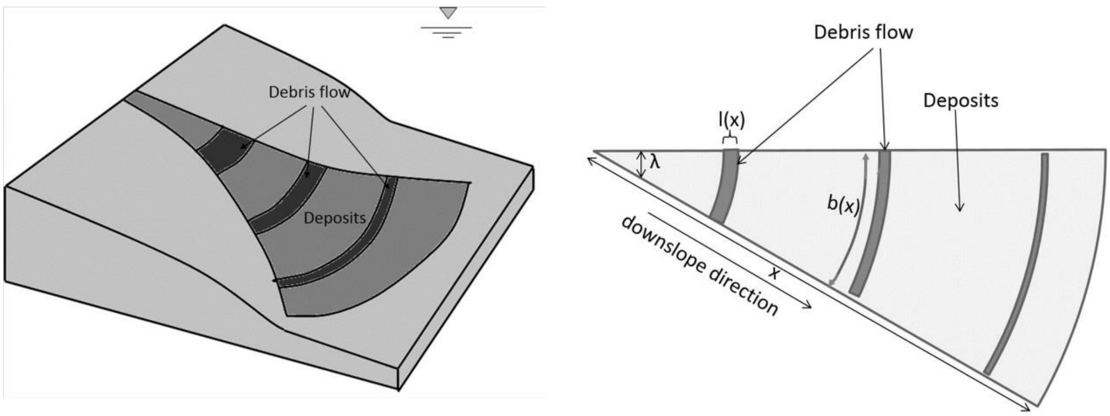

Figure 4. Plan view schematic of a slide on a gentle slope

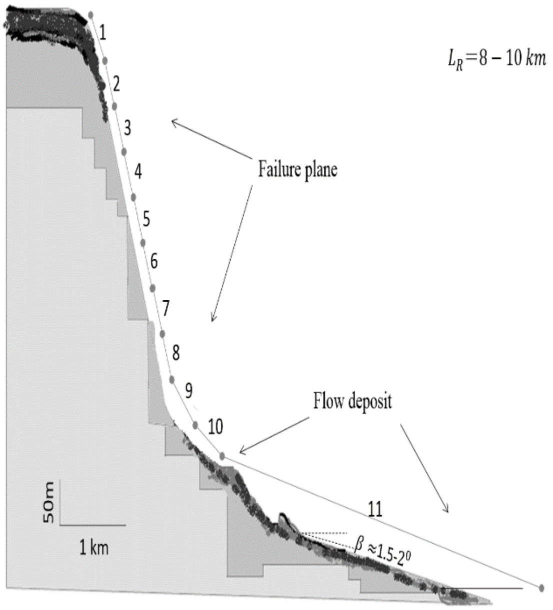

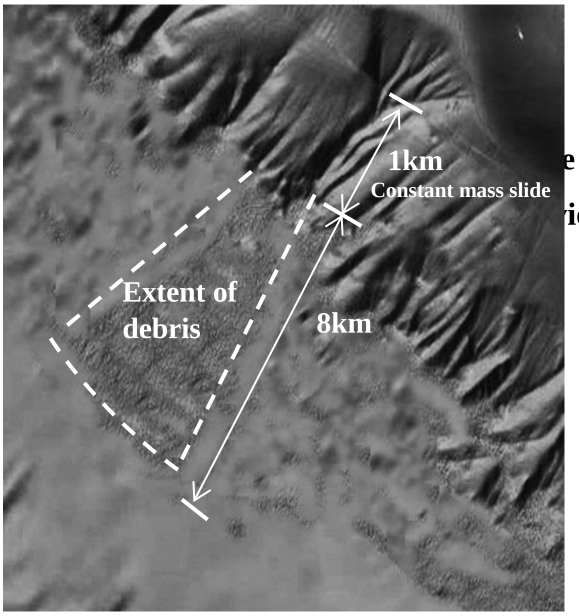

e Palos Verdes avalanche deposit: (a)
iew (after Locat et al., 2004)

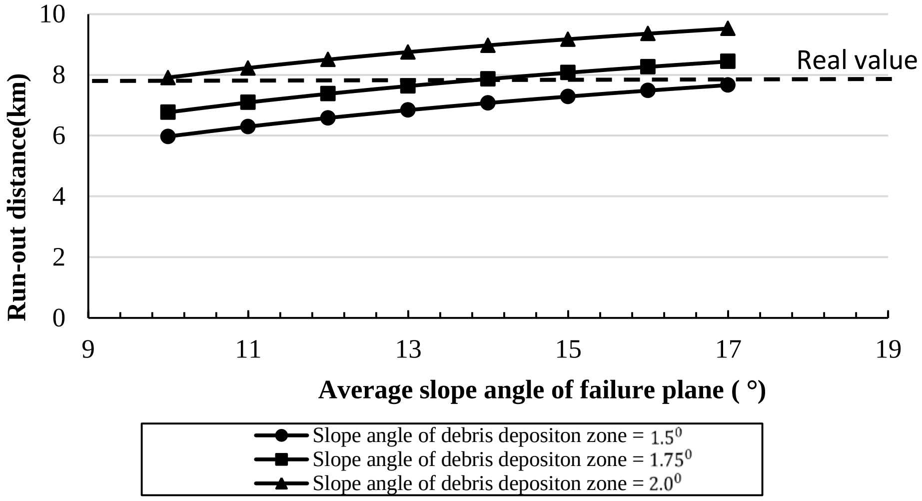
Real value
Run-out distance(km)
10
8
6
4
2
0
9
11
13
15
17
19
Average slope angle of failure plane (°)
Slope angle of debris depositon zone = 1.5^0
Slope angle of debris depositon zone = 1.75^0
Slope angle of debris depositon zone = 2.0^0

(a)

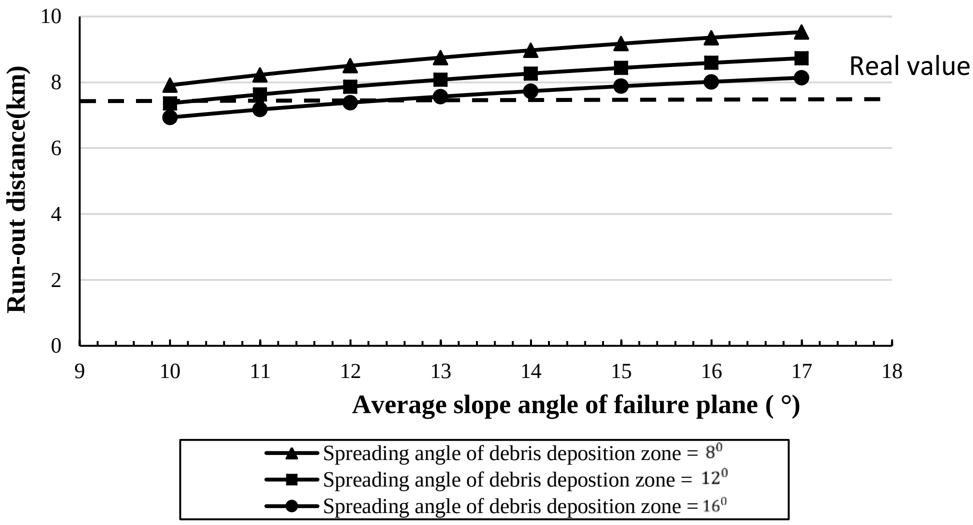
Real value
Run-out distance(km)
10
8
6
4
2
0
9
10
11
12
13
14
15
16
17
18
Average slope angle of failure plane (°)
Spreading angle of debris deposition zone = 8^0
Spreading angle of debris depostion zone = 12^0
Spreading angle of debris deposition zone = 16^0

(b)

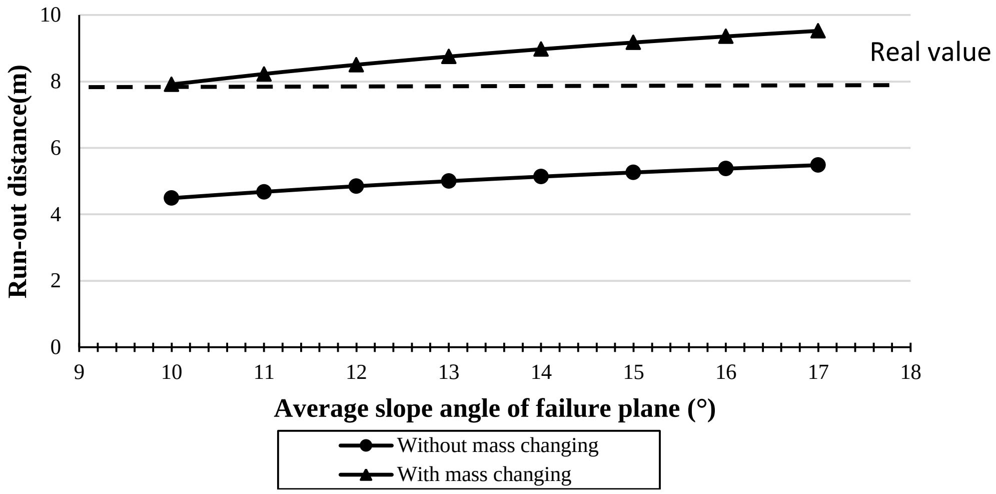

(c)

Figure 6. Calculated run-out distance: (a) with varying slope angles of the escarpment and the debris deposition zone; (b) with varying escarpment slope angles and spreading angles of the debris deposition zone; (c) with and without considering the mass changing model

Table 1 Geometry of escarpment for the Palos Verdes debris flow

Section ID	Length	Slope Angle	Section ID	Length	Slope Angle
1	0.1km	13.5°	7	0.1km	15.4°
2	0.1km	15.4°	8	0.1km	17°
3	0.1km	15.9°	9	0.1km	11.3°
4	0.1km	16.3°	10	0.1km	10°
5	0.1km	16.7°	11	unknown	1.75°
6	0.1km	16.2°			

Table 2 Parameters for analysis of the Palos Verdes debris flow

Unit weight of debris-flow material ($\boldsymbol{\rho_f}$)	25 $\mathrm{kN/m^3}$	Acceleration ($\dot{u}_{seismic}$)	0.35 g
Friction angle ($\boldsymbol{\alpha}$)	30°	Acceleration direction ($\boldsymbol{\theta}$)	10°
Average slope angle of escarpment ($\boldsymbol{\beta_1}$)	10–17°	Length of escarpment	1000 m
Slope angle of debris deposition zone ($\boldsymbol{\beta_2}$)	1.5–2°	Spreading angle of debris deposition zone ($\boldsymbol{\lambda}$)	8–16°
Initial length of moving block (l)	1000 m	Initial width of moving block ($\mathbf{b_0}$)	1000 m